

Nanoparticle Tracking Analysis of Polymer Nanoparticles in Blood Plasma

Mark S. Bannon, Aida López Ruiz, Karen Corrotea Reyes, Miriam Marquez, Zahra Wallizadeh, Mohammad Savarmand, Connor A. LaPres, Joerg Lahann, and Kathleen McEnnis*

A successful drug delivery system must overcome complex biological barriers. For particles injected into the blood, one of the first and most critical barriers pertains to blood stability to circulate through the human body. To effectively design drug delivery vehicles, interactions between the particles and blood, as well as the aggregation behavior, must be understood. This work presents a method to analyze particle size and aggregation in blood plasma using a commercially available nanoparticle tracking analysis (NTA) system. As a model system, fluorescently labeled polystyrene nanoparticles are incubated in goat blood plasma and analyzed using NTA. The particles incubated in plasma are found to have a protein corona that is larger than what has been observed by dynamic light scattering (DLS) in diluted plasma. Particles that are decorated with a PEG layer are also found to have large protein coronas in undiluted plasma. Because NTA is based on a unique visualization method, large multicomponent aggregates could be observed and quantified in a manner not feasible with other techniques. PEGylation of the particles is found to decrease the multicomponent aggregation from 1000 ± 200 particles for unmodified to 200 ± 30 particles for 1K PEGylated per 1×10^5 total particles.

1. Introduction

Targeted drug delivery has the potential to revolutionize medicine by increasing the efficacy of drugs while decreasing the unwanted side effects associated with them.^[1] Drug delivery can be an important treatment option for diseases such as cancer, where the toxicity of chemotherapy drugs limits the dosages.^[1] Despite numerous studies investigating drug delivery particles for cancer therapies, very few clinical products have resulted due


to the numerous biological hurdles that drug delivery particles must overcome.^[2–7]

The first hurdle faced by targeted drug delivery particles upon injection into the bloodstream is the need for circulation. In order to successfully deliver therapeutics to the correct part of the body, the particle must remain in circulation long enough to find the target. The circulation half-life depends on the interactions between the components in the blood and the particles themselves. Specifically, the adsorption of certain opsonins onto drug delivery particles leads to clearance of the particles from the bloodstream through phagocytosis.^[8–10] This rapid clearance directs the particles to the liver or the spleen instead of the intended target, resulting in failure of the drug therapy.^[4,9,11,12] Several strategies have been employed to improve particle circulation with the end goal being enhanced permeability and retention of the drug in question. One such strategy is PEGylation,

the attachment of polyethylene glycol (PEG) ligands.^[11,13,14] Additional methods include attachment of “markers of self” ligands and designed attachment to blood cells.^[15–18] Many drug delivery systems use particles between 10 and 100 nm in diameter to avoid this phenomenon; however, the interactions between blood and the particles typically cause a particle size increase, either through the formation of a protein corona or aggregation.^[5,19–24] This size increase greatly increases the number of particles removed from circulation before reaching the intended target.

M. S. Bannon, A. López Ruiz, K. Corrotea Reyes, M. Marquez, Z. Wallizadeh, M. Savarmand, Dr. K. McEnnis
Department of Chemical and Materials Engineering
New Jersey Institute of Technology
161 Warren St., Newark, NJ 07103, USA
E-mail: mcennis@njit.edu

M. S. Bannon
Department of Chemical Engineering
University of Virginia
395 McCormick Road, Charlottesville, VA 22903, USA

 The ORCID identification number(s) for the author(s) of this article can be found under <https://doi.org/10.1002/ppsc.202100016>.

© 2021 The Authors. Particle & Particle Systems Characterization published by Wiley-VCH GmbH. This is an open access article under the terms of the Creative Commons Attribution License, which permits use, distribution and reproduction in any medium, provided the original work is properly cited.

DOI: 10.1002/ppsc.202100016

C. A. LaPres, Prof. J. Lahann
Department of Chemical Engineering
University of Michigan
2800 Plymouth Rd, Ann Arbor, MI 48109, USA

Prof. J. Lahann, Dr. K. McEnnis
Biointerfaces Institute
University of Michigan
2800 Plymouth Rd, Ann Arbor, MI 48109, USA

Prof. J. Lahann
Department of Materials Science and Engineering
Department of Biomedical Engineering
Macromolecular Science and Engineering Program
University of Michigan
2800 Plymouth Rd, Ann Arbor, MI 48109, USA

Protein corona development and aggregation behavior of particles are typically determined by measuring particle size with dynamic light scattering (DLS).^[5,23–34] DLS requires a pure sample with monodisperse particles to ensure an accurate measurement of particles in the sample suspension.^[25] While some studies have found it is possible to measure particles in blood plasma using DLS, measuring particles directly in whole blood or even blood plasma is a difficult task, as the components of blood will scatter light as well.^[5,34,35] Thus, DLS measurements are only possible for certain size ranges of particles and with complex curve fitting. As a result, suspensions of particles in blood are often washed to remove the excess blood components, diluting the solution dramatically to measure the particles by DLS.^[5,27–32,35] While this technique allows for the accurate analysis of particle size after incubation in blood, it does not capture the actual environment that the particles encounter *in vivo*.^[9,19,35] Despite the need for a method to analyze particle behavior in blood plasma, there are very few reports on particle behavior in these environments.^[25,34,36–40] This article uses nanoparticle tracking analysis (NTA) to investigate the behavior of polystyrene (PS) particles in blood plasma. This method uses the fluorescently labeled particles to reduce the effects of scattered light from the components of blood plasma. Fluorescent particle analysis in blood plasma has been shown to be successful in methods such as fluorescence correlation spectroscopy^[38] and fluorescence single particle tracking,^[36] and NTA provides an alternative approach.^[25,35] NTA eliminates the need for a monodisperse selection of particles within analyzed samples, allowing for interactions to be measured between particles and blood. Upon analysis, a substantial protein corona, much larger than measured by DLS, is found to form on the particles in blood plasma, and large multicomponent aggregates are observed and quantified.

2. Results

2.1. Measuring Nanoparticles in Blood Plasma

Using fluorescent particles enables the observation of interactions between particles and blood plasma. While in fluorescent mode, the amount of scattered light captured by the microscope is decreased, requiring an increase in the camera level used by the image (Figure S1, Supporting Information). Scatter mode, on the other hand, observes all light scattered by all components in the system, whether polystyrene, blood components, or even dust and debris. **Figure 1** shows the progression of the observation of a sample in scatter mode to fluorescent mode.

Figure 1a shows the observed light from a scatter mode analysis of a sample of PS particles in blood plasma. The blue pixels represent points of saturated scattered light; however, it is almost impossible to visually determine the PS particles from debris within the sample. NTA also cannot specifically analyze the scattered light from the PS particles in these videos. Figure 1b displays the observed light from blood plasma without added PS particles analyzed using “fluorescent mode” on the Malvern Nanosight NS300 NTA system, while Figure 1c shows the observed light from a blood plasma sample with added fluorescently labeled PS particles. Figure 1b,c shows a

noticeable decrease in observed light, as the light scattered by various debris and blood components in the sample is blocked by the fluorescent filter. Figure 1b shows that the blood plasma itself has little to no background fluorescence, meaning that the points of light seen in Figure 1c are exclusively from the fluorescently tagged PS particles. Figure 1 proves that the fluorescent capabilities of NTA allow for analysis of PS particles in blood plasma without a considerable dilution of the sample.

2.2. Comparison with DLS

To compare the size results attained from NTA with those from DLS, blood plasma or serum must be diluted such that the scattered light intensity from the particles is greater than the scattered light intensity from the components of the blood plasma. To achieve this, the unmodified PS particles were incubated in blood plasma and then diluted with saline solution to various dilutions. The particles were then analyzed using NTA, and when the solutions were dilute enough, they were also analyzed with DLS. This experiment was also completed using PS particles incubated in pure saline solution to provide a standard for size of the PS particles. **Figure 2a** shows the size analysis results from NTA of PS particles incubated in two different batches of goat blood plasma dilutions and pure saline solution, in which the mode hydrodynamic diameter of particles in each dilution is plotted against the dilution factor on a logarithmic scale. The dilution factor is calculated as the final volume of the diluted measurement solution divided by the volume of the initial incubation solution. Figure 2b shows the size analysis results of the same PS particles incubated in pure saline and then measured using DLS, in which the intensity of the light is plotted against the hydrodynamic diameter of the particles on a logarithmic scale. Figure 2c depicts the same PS particles measured in blood plasma at different dilutions using both NTA and DLS. Like Figure 2a, Figure 2c plots the mode hydrodynamic diameter of particles in each dilution against the dilution factor on a logarithmic scale.

The results of the protein corona dilution experiments in Figure 2a show that as the blood plasma solutions become more dilute with a higher dilution factor, the measured hydrodynamic diameters of the particles decrease. The error bars in Figure 2 represent the standard deviation and these same plots are displayed with standard error in the supplemental information (Figure S2, Supporting Information). The measured hydrodynamic diameter of the particles in concentrated blood plasma was proven to be statistically different than the hydrodynamic diameter in the most diluted blood plasma by a single factor analysis of variance test (ANOVA) and a Games-Howell pairwise comparison for both sets of blood plasma in Figure 2a (Figures S3 and S4, Supporting Information). NTA provides a standard error of less than 5 nm per each data point in Figure 2a, giving accurate size measurements for each dilution. In Figure 2a, the PS particles in saline did not display a statistically different size across each dilution, as proven by single-factor ANOVA Games-Howell pairwise comparison, demonstrating that the dilution method did not affect the hydrodynamic diameter of the particles (Figure S5, Supporting Information).

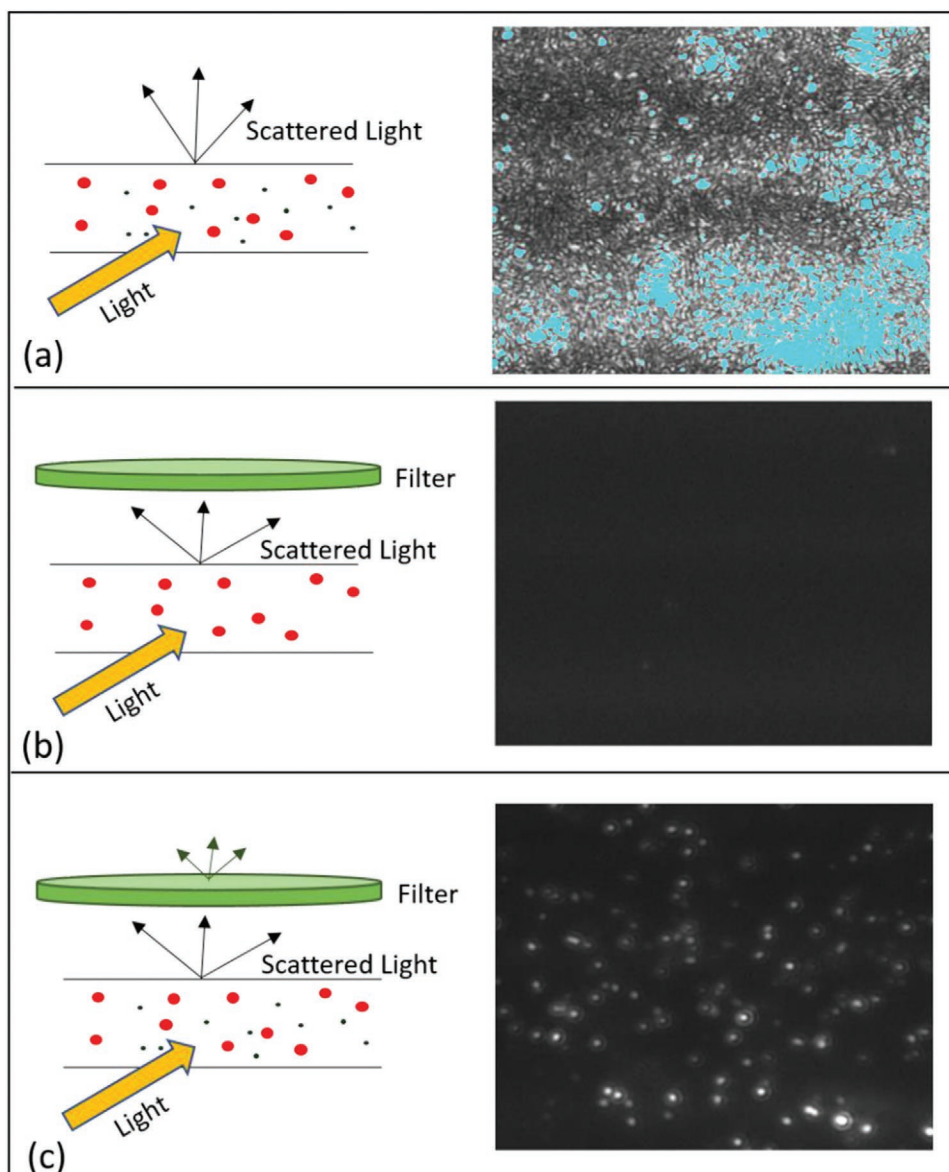


Figure 1. Schematics and results from NTA of carboxyl-PS nanoparticles in blood plasma. a) Schematic showing the unfiltered scattering of light in scatter mode (Left). PS nanoparticles as well as components in blood plasma scatter light, leading to an increased and non-selective signal being sent to the detector (right). b) Schematic showing the filtered scattering of light in fluorescent mode (left). Only light scattered at wavelengths above the fluorescent filter get received by the detector, where the lack of any fluorescent tagging leads to an extremely low signal (right). c) Schematic showing the filtered scattering of light in fluorescent mode (left). PS nanoparticles can be fluorescently tagged in order to emit light that can permeate the fluorescent filter, creating a selective visual result that only detects the tagged carboxyl PS particles (right).

Figure 2b demonstrates the clear and concise measurements given by DLS when measuring the PS particles in pure saline solution. In contrast, DLS measurements obtained from particles incubated in blood plasma were considered “of too poor quality for cumulative analysis” unless diluted to the lowest concentration used in this study, a dilution factor of 512 corresponding to approximately 0.07% blood plasma. Due to the residual blood components present in higher concentrations of blood plasma, accurate particle sizes could not be interpreted; therefore, the only reportable DLS measurement in blood plasma came from a dilution factor of 512, as seen in Figure 2c. The reported size of the particles from DLS at a

dilution factor of 512 agree with the NTA reported size at the same dilution.

2.3. Particle PEGylation

Polyethylene glycol (PEG) is often attached to particles utilized in drug delivery to make use of its “stealth” properties to decrease interactions between the particles and blood components.^[11] To demonstrate these effects, PS particles were PEGylated with PEG of different molecular weights: 1000 g mol⁻¹ (1K), 5000 g mol⁻¹ (5K), 10 000 g mol⁻¹ (10K) and 30 000 g mol⁻¹

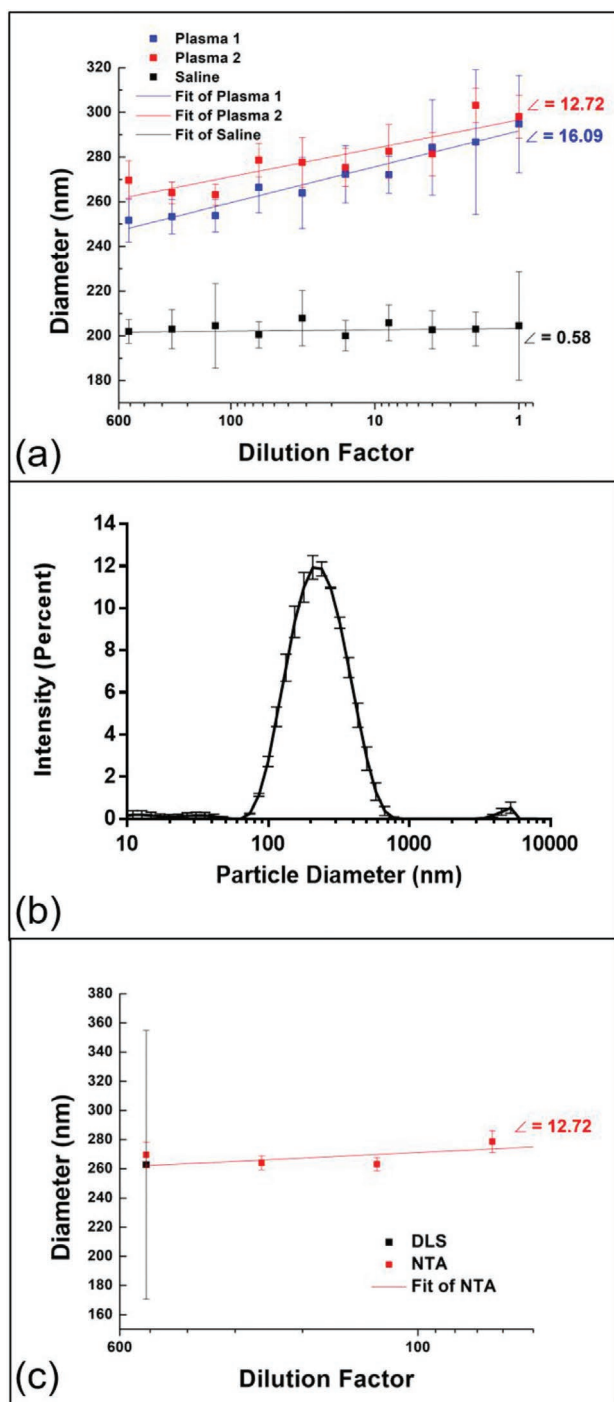


Figure 2. a) NTA measurements of PS particles incubated in saline (black) and two batches of goat blood plasma (red, blue) and subsequently diluted. For saline measurements, the initial amount of blood plasma was replaced with saline. Displayed error bars represent standard deviation for each data set. b) DLS measurement of PS particles in pure saline. Displayed error bars represent standard deviation for each data set. c) Comparison of results using both NTA and DLS of measurements of PS particles incubated in blood plasma and subsequently diluted using saline. DLS measurements in solutions with dilution factors less than 512 were reported as “too poor for cumulative analysis”, and were omitted from the figure. Displayed error bars represent standard deviation for each data set.

(30K). **Figure 3a** displays the size distribution of the hydrodynamic diameters of the unmodified PS particles when incubated in saline compared to the same particles incubated in plasma. The normalized concentration of the particles against their respective sizes is reported to compare the size distribution in saline to that in plasma. The corresponding size distribution graphs for the PEGylated particles are reported in **Figure S6** (Supporting Information). While this experiment was repeated many times for each type of PEGylation, these results only show one representative individual NTA run. For each PEGylation, the particles experience a noticeable size increase upon incubation in plasma compared to incubation in saline from the development of a protein corona.

Table 1 reports the thicknesses of the protein coronas developed on the different PEGylated particles: unmodified, 1K PEGylated, 5K PEGylated, 10K PEGylated, and 30K PEGylated. DLS confirmed successful PEGylation by showing an increase in zeta potential on PEGylated PS particles compared to the negative zeta potential of the unmodified carboxylate-PS particles (**Figures S7 and S8**, Supporting Information). Transmission electron microscopy (TEM) was also used to display a PEG layer on the surface of PEGylated PS particles (**Figure S9**, Supporting Information). As displayed by the schematic in **Figure 3b**, the protein corona thickness is calculated by subtracting the measured hydrodynamic diameter of the particle in saline (the size of the PS particle with no protein corona) from the measured hydrodynamic diameter of the particle in plasma and dividing by 2.^[27] There is approximately an 11 nm range between the thickest protein corona and the thinnest, which develop on the 1K and 30K PEGylated particles, respectively. The 1K PEGylated particles developed the thickest protein corona (72 ± 36 nm) and the 30K PEGylated particles developed the thinnest (61 ± 16 nm); however, a single factor ANOVA and Games-Howell pairwise comparison on this data proved that the developed protein coronas on the 1K and 30K PEGylated particles did not have statistically different thicknesses (**Figure S10**, Supporting Information). The protein corona developed on unmodified polystyrene particles is 63 ± 17 nm. The developed protein corona accounts for approximately a third of the total size of the particles.

2.4. Homogeneous Aggregation

It is well known that the presence of salt can cause aggregation between particles (homogeneous aggregation) in solution because the salt screens the charges on the particles, and thus the charge repulsion between particles decreases. Since blood contains a relatively high salt content, particles were first tested in normal saline for homogeneous aggregation behavior. PS particles with different surface functional groups (sulfate, carboxylate, or amine) were incubated in saline and analyzed for the presence of homogeneous aggregation. PS particles with sulfate functional groups were found to readily aggregate after brief incubation with normal saline, while PS particles decorated with amine functional groups showed some aggregation in both saline and water. Carboxylate PS particles did not appear to aggregate in normal saline (**Figure S11**, Supporting Information) as the size distribution in water and saline are

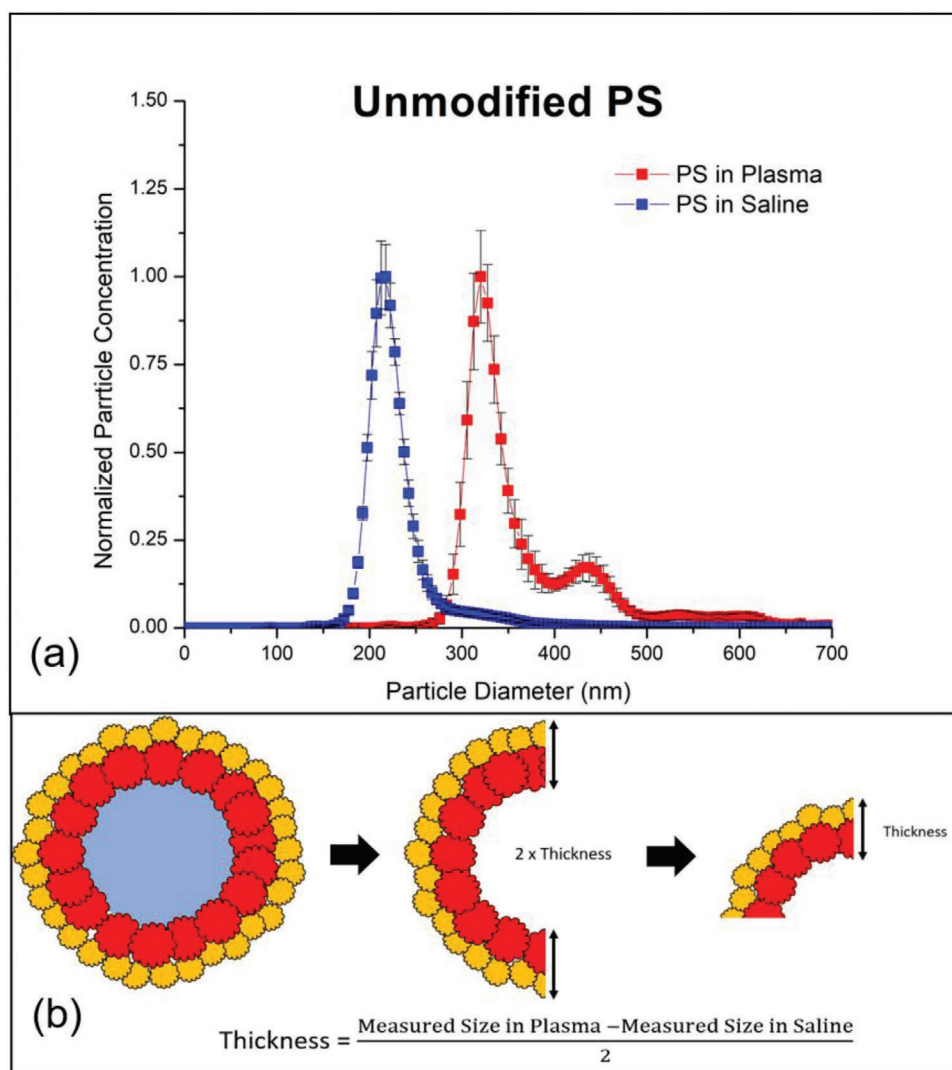


Figure 3. a) NTA size distribution plot of unmodified PS particles in saline and blood plasma. The displayed size disparity between particles incubated in saline and plasma confirms the presence of a protein corona. Displayed error bars represent the standard error for each data set. b) Schematic justification of protein corona thickness calculations. The difference between the measured hydrodynamic diameter of PS particles in plasma and saline is equal to twice the thickness of the protein corona, which can be halved to give us the effective corona thickness.

Table 1. Mode hydrodynamic diameters of PS particles with various PEGylations in saline and blood plasma measured by NTA. Includes calculated protein corona thickness of the particle variants in goat blood plasma. Displayed error represents standard deviation for each data set. Data with standard error presented in Table S3 (Supporting Information).

PS particle modification	Mode hydrodynamic diameter in saline [nm]	Mode hydrodynamic diameter in goat blood plasma [nm]	Calculated protein corona thickness in goat blood plasma [nm]
Unmodified	196.1 ± 3.2	322.3 ± 16.9	63.1 ± 17.2
1K PEGylated	209.0 ± 15.7	353.8 ± 33.1	72.4 ± 36.7
5K PEGylated	208.6 ± 5.9	338.2 ± 18.4	64.8 ± 19.4
10K PEGylated	216.1 ± 8.0	354.8 ± 29.4	69.3 ± 30.5
30K PEGylated	244.7 ± 5.1	366.3 ± 15.7	60.8 ± 16.5

similar. For this reason, PS-carboxylate particles were used for further experiments in blood plasma.

2.5. Multicomponent Aggregation

NTA provides the ability to visually confirm the occurrence of multicomponent aggregation upon particle incubation in blood plasma. **Figure 4a** displays a screenshot of a large multicomponent aggregate of particles moving through blood plasma. This aggregate is confirmed as a multicomponent aggregate because of its motion, represented by the blue tracking lines following the particles. The blue lines describing the motion of particles in the multicomponent aggregate are straight, with very little variation in direction and all the particles in the aggregate moving in the same manner. Conversely, individual particles have very erratic motion paths, which is shown by the

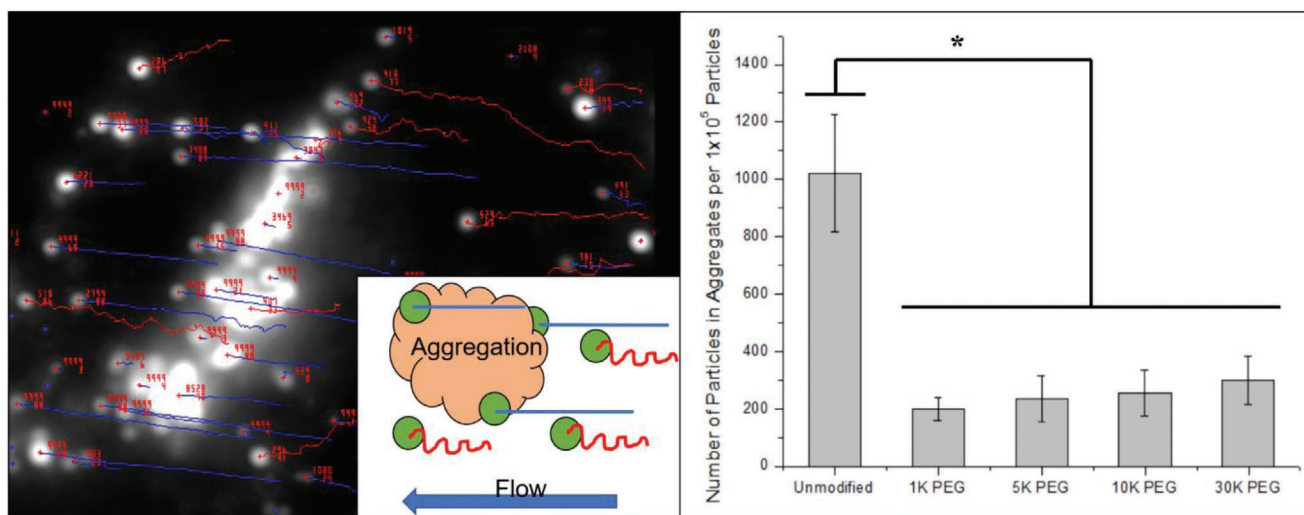


Figure 4. Presence of large multicomponent aggregates of particles in blood plasma appear in NTA videos. a) Screenshot of NTA of carboxylate-PS nanoparticles in goat blood plasma during video processing. Particle tracks are represented by the blue and red lines. Particles in multicomponent aggregates have relatively straight particle paths compared to individual particles. Schematic of a multicomponent aggregate with particle tracks is depicted in the bottom right corner. b) Quantification of number of particles in multicomponent aggregates per 1×10^5 particles over 24 h of incubation in goat blood plasma. Displayed error bars represent standard error for each data set.

red tracking lines describing their motion. By comparing the movement of particles in the videos, a number of particles in multicomponent aggregates can be quantified. A multicomponent aggregate was defined as containing at least two particles that were moving together without the “wiggle” of Brownian motion. Multicomponent aggregates can be differentiated from homogeneous aggregates as a particle aggregating with another particle would appear as a larger, brighter dot in the videos and not separate dots moving in the same manner as described here. Figure 4b quantifies the total number of particles in multicomponent aggregates per 1×10^5 total particles that developed over a 24 hour period of particle incubation in plasma. There is a significant decrease in the number of particles that form multicomponent aggregate found in the suspensions of unmodified particles than those of PEGylated particles (Figure S12, Supporting Information). The highest number of particles in multicomponent aggregates observed was approximately 1000 ± 200 particles per 1×10^5 particles in the unmodified particle suspensions. The least amount of particles in multicomponent aggregates observed was approximately 200 ± 30 particles per 1×10^5 particles in the 1K PEGylated particle suspensions. There was not a statistical difference in the normalized number of particles in multicomponent aggregations between the different PEGylated particle groups.

3. Discussion

NTA can characterize particle behavior in blood plasma, and the results of the dilution and aggregation experiments validate that it is possible to measure this behavior in undiluted blood plasma.^[5,25,35] Due to the use of Alsever’s solution as the anticoagulant, the highest blood plasma solution tested in this study was a 35.5% dilution of blood plasma and isotonic salt solution (dilution factor 0), making the lowest dilution 0.07%

blood plasma (dilution factor 512). A table corresponding the dilution factor to approximate blood plasma percentage is available in Table S1 (Supporting Information). An anticoagulant is necessary to prevent clotting from occurring during the experiment, but by using other types of anticoagulant, higher blood plasma concentrations can be achieved. For instance, using bovine blood plasma with sodium citrate as the anticoagulant results in a maximum blood plasma concentration of 96% and particles can still be analyzed at these concentrations with minimal background noise (Figure S13, Supporting Information). At the same time, particle hydrodynamic diameter measurements using DLS in solutions containing higher than 0.07% blood plasma were inconclusive, as the presence of blood plasma components made it difficult to determine the signal from the particles.

Upon increasing dilution of the blood plasma with saline, the hydrodynamic diameters of the particles decreased as their corresponding solutions became more dilute. According to the hard/soft protein corona model, the proteins in the loosely bound soft corona more readily desorb and adsorb from the particle surface.^[21,34] As more saline is added, the equilibrium shifts toward more proteins in the soft corona desorbing than adsorbing, causing an incremental decrease in the hydrodynamic size that is observed as more saline is added to the particles after incubation.^[22,33] As more saline is added, many of the proteins contributing to the soft protein corona are being washed off of the particles, which causes the observed size decrease in the NTA results in Figure 2a. DLS data can only be obtained at a dilution factor of 512, where it agrees with NTA data at that blood plasma concentration. The size measured by NTA at the dilution factor of 512, however, is significantly different than the size measured by NTA at the highest concentration tested (Figures S3 and S4, Supporting Information). A difference of approximately 30 nm exists between the particle diameters in the two extremes of blood plasma concentration.

The highest plasma concentration tested is a more accurate representation of the particle size and protein corona size the particle would have in the body.

An alternative explanation to the increase in particle size with increasing blood plasma concentration could be the depletion effect, the phenomenon where the surface area of the particles is unavailable to blood plasma proteins due to overcrowding of particles in solution. Theoretically, this would attribute the increase in measured size of the particles through NTA not to the protein corona, but to the particle concentration increase in incubation solution for each subsequent dilution. Despite this possibility, Figure 2a demonstrates that the depletion effect is not occurring in these experiments. There is a very clear increase in the y-intercept of the fitted equations describing the hydrodynamic diameter trend of particles incubated in blood plasma compared to those incubated in pure saline. In the lowest percent plasma measurements (where particle concentration in the plasma during incubation is highest), this difference still exists, and the size of the measured particles only increases from there. Because such a large difference in size is observed between a dilution factor of 512 and pure saline, it can confidently be stated that proteins are being bound to the nanoparticle surface, forming the hard corona. The increase in size with increasing blood plasma concentration can then be attributed to the soft protein corona, and not the depletion effect.

The use of NTA to analyze particles in blood plasma allows for the testing of various particle surface chemistries and their effects on the protein corona. It was expected that 1K, 5K, 10K, and 30K PEGylated particles should have smaller protein coronas than the unmodified particles; however, the calculated protein corona thicknesses derived by NTA measurements in Table 1 show little change.^[8,11] This behavior could be attributed to the inclusion of the soft protein corona in NTA measurements. The soft protein corona is comprised of loosely bound proteins; therefore, the flow rate of the particle suspension through the microfluidic viewing device of the NTA will have a significant effect on the soft protein corona. Varying the flow rate will vary the shear force applied to the nanoparticles and, therefore, the adherence of soft corona proteins to the PS particles, ultimately leading to the derived particle size in plasma, and total protein corona thickness, to be dependent on the sample flow through the microfluidic device (Figure S14, Supporting Information). As blood flow rate can vary in the body, it is important to analyze protein corona development under flow.

Using DLS, particles must either be washed or measured in filtered or diluted plasma or serum, producing reported protein corona thicknesses in the literature less than 40 nm on polystyrene particles.^[28–30,38] This is much smaller than the 63 ± 17 nm thick protein corona measured in 35.5% plasma solution in this study, yet comparable to the 24 ± 13 nm thick protein corona measured at a dilution factor of 512. The DLS protein corona measurements in literature have larger errors than those obtained by NTA, and only represent the hard protein corona since DLS is unable to represent the effects of undiluted plasma or serum on particles.^[28–30] The observed protein corona developed on the various PEGylated particles in this study was between 61 and 72 nm thick. This measurement was also significantly larger than protein coronas on PEGylated particles measured by DLS in literature, which vary between 5 and

40 nm thick (depending on surface charge and original particle size).^[27,31,32] The reports in the literature represent measurements of the hard protein corona after washing or measurements in filtered or diluted plasma, serum, or plasma protein solution, and therefore are unable to characterize the full developed protein corona in undiluted plasma.^[35]

While beyond the scope of this paper, efforts have been made to characterize the composition of the protein corona. The literature shows the hard protein corona on polystyrene nanoparticles to be primarily made of apolipoprotein AI, human serum albumin, fibrinogen, IgG, transferrin, and inter-alpha-trypsin inhibitor heavy chain, among others.^[30,39–42] It has also been found that nanoparticle PEGylation can affect the protein corona composition.^[41,42] Additionally, efforts have been made to characterize the adsorption rates of various proteins onto nanoparticles in various complex biological milieu, which can be done through fluorescence correlation spectroscopy,^[43–46] and nuclear magnetic resonance spectroscopy,^[46] among others.^[37] The protein corona is an integral factor in cell uptake of nanoparticles; therefore, both the protein composition and binding kinetics should be considered when formulating nanoparticle drug delivery systems.

By observing the particles in blood plasma over time, this method shows that the interactions between particles and blood plasma not only lead to a particle size increase, but they can also cause multicomponent aggregation of particles and plasma components. As displayed by the error bars in Figure 4b, there is no statistical significance between the normalized number of particles in aggregates for any one surface modification of the particles; however, the statistical difference between the 1K, 5K, 10K and 30K PEGylated PS particles in aggregates and the unmodified PS particles in aggregates is a clear indication that manipulating the surface of drug delivery vehicles decreases the multicomponent aggregation of particles in plasma (Figure S11, Supporting Information).

4. Conclusion

There is a clear need to increase our understanding of how the human body interacts with materials, especially in the field of targeted drug delivery. Using NTA to analyze particles in blood plasma provides helpful insight into how blood components affect the size and aggregation behavior of drug delivery vehicles injected into undiluted blood plasma that cannot be studied by other methods which require extensive dilution or washing and remove the soft protein corona. Information from these experiments will allow for the optimization of different tunable surface properties, such as PEGylation. With a method now in place for experiments using NTA in blood plasma, different properties of the vehicles can be explored to further understand and design particles to create the most effective and most efficient circulation of targeted drug delivery vehicles through the bloodstream.

5. Experimental Section

Blood Plasma Preparation: Whole goat blood treated with the anticoagulant Alsevers solution was ordered from Lampire Biological

Laboratories (catalog# 7202503). Upon receipt (3 d after the blood was drawn), the whole blood was centrifuged at 2000 RCF for 10 min and the blood plasma was separated from the blood cells. The centrifugation procedure was repeated 3 times to remove all the blood cells. Kinematic viscosity measurements were made on the blood plasma and all blood plasma dilutions using a glass capillary Ubbelohde viscometer (Fisher Scientific catalog# 13614F) in a water bath at 37 °C. Kinematic viscosity values used were the average of 10 measurements. To convert this to dynamic viscosity, the density of blood plasma needs to be taken into account. Human blood plasma density can be approximated to 1.0025 g cm⁻³, while Alsever's solution can be approximated to the same as a 90% medical saline solution, or 1.0046 g cm⁻³. Taking these values into account, the density of blood plasma was approximated to be 1.0000 g cm⁻³, after concluding that the error in the size measurements from the NTA was larger than the error created by the density assumption.

Dilution Experiment: FluoSpheres carboxylate-modified polystyrene nanoparticles 200 nm in diameter labeled with a yellow-green dye (excitation 505 nm, emission 515 nm) were purchased from ThermoFisher (catalog# F8811). 100 µL of the as-received particle solution was diluted with 900 µL of normal saline to create a solution with a concentration of particles ready to be used in experiments. The PS particles from this solution were incubated in various amounts of plasma for 10 separate dilutions with the amount of plasma being incrementally halved for each dilution. For each dilution, the designated amount of plasma was pipetted into a 2 mL Eppendorf tube, followed by an amount of diluted particle solution, the concentration of which being adjusted to give the ideal concentration range for NTA analysis of around 8 × 10⁸ particles per ml. The tube was vortexed for 10 seconds and placed into a water bath uniformly set to 37 °C (in order to simulate the temperature conditions of the human body) and left to incubate for 10 min.

After the incubation period, the appropriate amount of saline, also warmed to 37 °C, was added to the sample and the tube was vortexed again for 10 s. Each sample was loaded into a Malvern NanoSight NS300 to be pumped continuously through the microfluidic viewing device with a syringe pump and measured. The temperature inside the chamber of the Nanosight NS300 that held the sample was held constant at 37 °C. The syringe pump was set to an appropriate flow rate such that the particles took approximately 5–10 s to pass the viewing area (equivalent to a flow rate of 100 au on the specific system used for many of the measurements, though this number varied on different instruments). The instrument was set to take in between seven and ten videos for each measurement, with each video lasting 60 s. The solutions were analyzed using a 488 nm laser with the Nanosight NS300 set to fluorescent mode using a 500 nm fluorescent filter. Each dilution was created three times and then ran through the Nanosight NS300 as described above.

Analysis of the resulting videos was done using the NTA 3.2 software provided by Malvern. The threshold was set such that most of the particle centers were detected and a minimum amount of background noise was detected. The resulting data on particle tracking and size was checked for vibration errors. Any runs labeled as “high vibration” by the software were thrown out and not included in the averages. Only measurements that had 4 or more runs without a high vibration error were included for size analysis and measurements without at least 4 useable runs were repeated. The resulting particle sizes were adjusted for viscosity by multiplying the reported particle diameter by the ratio of the viscosity of pure water at 37 °C (the default viscosity used for calculation by the Nanosight NS300) to the measured viscosity of the blood plasma.

Particle PEGylation: PS particles were pegylated using amine-functionalized 1k linear PEG (Nanocs cat#PG1-AM-1k), 5k linear PEG (Nanocs cat#PG1-AM-5k), 10k linear PEG (Nanocs cat#PG1-AM-10k), and 30k linear PEG (Nanocs cat#PG1-AM-30k). 1-ethyl-3-(3-dimethylaminopropyl) carbodiimide hydrochloride (EDC)/sulfo-N-hydroxysuccinimide (NHS) chemistry was used to attach the amine-modified PEG to the carboxylic acid functionalized particles. To do this, 1 mL of 2 × 10⁻³ M EDC in 2-(N-morpholino)ethane sulfonic

acid (MES) buffer was added to 50 µL of PS particles (as received). The solution was then briefly vortexed and allowed to react for 10 min at room temperature on a rotator while covered in foil. Next, sulfo-NHS was added to a concentration of 5 × 10⁻³ M and allowed to react for 10 min at room temperature on a rotator while covered in foil.

The samples were centrifuged at 21130 RCF for 1 h and the supernatant was removed. The particles were dispersed in PBS by tip sonication at 20% power on ice, using 1 s pulses with 5 s in between each pulse five times for a total of 5 s of pulse time. 10 mg of each type of PEG was then added to the PBS/activated particle solution. The sample was briefly vortexed and allowed to react for 2 h at room temperature on a rotator while covered in foil.

The particle solution was again centrifuged at 21130 RCF for 1 h, the supernatant was removed and saline was added. The sample was centrifuged and washed with saline two more times. On the final wash, the particles were again dispersed in saline to a total volume of 1 mL. Finally, dilutions were then measured in the NTA in order to determine particle size and concentration.

PEGylation of the particles was studied by measuring Z-potential. For that, a solution of 1 mL of each of the samples with a minimum concentration of particles of 10⁹ particles mL⁻¹ was used. By measuring z-potential with a Zetasizer nano ZS, Malvern Instrument, it was possible to compare unmodified particles and PEGylated ones.

PEGylation of PS-particles was also characterized by FEI Tecnai G2 Spirit Twin Transmission Electron Microscopy (TEM) at an operating voltage of 120 kV. For the sample preparation, particles were dried on 300-mesh copper-coated grids with a carbon film purchased from Electron Microscopy Science. Samples were stained with uranyl acetate to increase the contrast of the polymer.

Homogeneous Aggregation Experiment: FluoSpheres polystyrene nanoparticles 200 nm in diameter labeled with a yellow-green dye (excitation 505 nm, emission 515 nm) that were either carboxylate-modified, amine-modified, or sulfate-modified were purchased from ThermoFisher (catalog# F8811, #F8764 and #F8848). 10 µL of the as-received particle solution was diluted with 1 mL of normal saline or water. 100 µL of diluted particle solution was added to 10 mL of saline or water. 1 mL of the solution was removed and NTA measurements were done on the Nanosight NS300 at 37 °C using a 488 nm laser and 500 nm long-pass filter.

Multicomponent Aggregation Experiment: A sample of PS particles was incubated in plasma and placed on a tube rotator in an incubator at 37 °C. A sufficient amount of particle solution was added in order to have a concentration of 8 × 10⁸ particles per mL of solution for ideal analyzing conditions for NTA. After 10 min of incubation, a 1 mL sample of the particles in plasma was analyzed using NTA on the Nanosight NS300 for the “0 h” measurement and measured in the same manner as described in the “Dilution Experiment” section.

The particles were incubated in the blood plasma continuously for 24 h inside of the incubator. A 1 mL sample of solution was removed to be measured at 0, 4, 9, 12, 15, 18, 21, and 24 h. The videos of fluorescently tagged particles moving through the plasma were then viewed and analyzed in order to count the total number of particles that aggregated in each video for each type of PS particles. These numbers were compared to the total number of particles counted in the video, as reported by the NTA software, and normalized results comparing the number of particles in aggregates per 1 × 10⁵ particles were calculated across samples. A normalization to 1 × 10⁵ particles was chosen in order to account for any differences in concentration of particles across measured samples. For each particle type, the number of particles in aggregates per 1 × 10⁵ particles were averaged across each time point and error bars represent the standard error between time points.

Supporting Information

Supporting Information is available from the Wiley Online Library or from the author.

Acknowledgements

The authors thank Kourtney Gans, Alison Shweh, Andressa dos Santos Moreira, Janki Patel, Sean McLoughlin, David Burkland, and Abbi Bader for their help with data acquisition and analysis.

Conflict of Interest

The authors declare no conflict of interest.

Data Availability Statement

Data available on request from the authors.

Keywords

nanoparticle tracking analysis, particle aggregation, polystyrene nanoparticles, protein corona

Received: March 31, 2021

Revised: April 23, 2021

Published online: May 19, 2021

- [1] S. Senapati, A. K. Mahanta, S. Kumar, P. Maiti, *Signal Transduction Targeted Ther.* **2018**, *3*, 7.
- [2] I. Brigger, C. Dubernet, P. Couvreur, *Adv. Drug Delivery Rev.* **2012**, *64*, 24.
- [3] M. Ferrari, *Nat. Rev. Cancer* **2005**, *5*, 161.
- [4] H. Gao, Q. He, *Expert Opin. Drug Delivery* **2014**, *11*, 409.
- [5] K. Rausch, A. Reuter, K. Fischer, M. Schmidt, *Biomacromolecules* **2010**, *11*, 2836.
- [6] T. Sun, Y. S. Zhang, B. Pang, D. C. Hyun, M. Yang, Y. Xia, *Angew. Chem.* **2014**, *126*, 12804; *Angew. Chem., Int. Ed.* **2014**, *53*, 12320.
- [7] A. Wicki, D. Witzigmann, V. Balasubramanian, J. Huwyler, *J. Controlled Release* **2015**, *200*, 138.
- [8] R. Gref, M. Lück, P. Quellec, M. Marchand, E. Dellacherie, S. Harnisch, T. Blunk, R. Müller, *Colloids Surf., B* **2000**, *18*, 301.
- [9] T. M. Göppert, R. H. Müller, *Int. J. Pharm.* **2005**, *302*, 172.
- [10] D. Owens, N. Peppas, *Int. J. Pharm.* **2006**, *307*, 93.
- [11] J. L. Perry, K. G. Reuter, M. P. Kai, K. P. Herlihy, S. W. Jones, J. C. Luft, M. Napier, J. E. Bear, J. M. DeSimone, *Nano Lett.* **2012**, *12*, 5304.
- [12] H. Zou, Z. Wang, M. Feng, *J. Controlled Release* **2015**, *214*, 121.
- [13] A. A. D'souza, R. Shegokar, *Expert Opin. Drug Delivery* **2016**, *13*, 1257.
- [14] J. Liu, M. Yu, X. Ning, C. Zhou, S. Yang, J. Zheng, *Angew. Chem.* **2013**, *125*, 12804; *Angew. Chem., Int. Ed.* **2013**, *52*, 12572.
- [15] P. L. Rodriguez, R. Harada, D. A. Christian, D. A. Pantano, R. K. Tsai, D. E. Discher, *Science* **2013**, *339*, 971.
- [16] E. Chambers, S. Mitragotri, *Exp. Biol. Med.* **2007**, *232*, 958.
- [17] J. S. Brenner, D. C. Pan, J. W. Myerson, O. A. Marcos-Contreras, C. H. Villa, P. Patel, H. Hekierski, S. Chatterjee, J. Q. Tao, H. Parhiz, K. Bhamidipati, T. G. Uhler, E. D. Hood, R. Y. Kiseleva, V. S. Shuvaev, T. Shuvaeva, M. Khoshnejad, I. Johnston, J. V. Gregory, J. Lahann, T. Wang, E. Cantu, W. M. Armstead, S. Mitragotri, V. Muzykantov, *Nat. Commun.* **2018**, *9*, 2684.
- [18] U. Prabhakar, H. Maeda, R. K. Jain, E. M. Sevick-Muraca, W. Zamboni, O. C. Farokhzad, S. T. Barry, A. Gabizon, P. Grodzinski, D. C. Blakey, *Cancer Res.* **2013**, *73*, 2412.
- [19] V. Mirshafiee, R. Kim, M. Mahmoudi, M. L. Kraft, *Int. J. Biochem. Cell Biol.* **2016**, *75*, 188.
- [20] R. M. Pearson, V. V. Juetner, S. Hong, *Front. Chem.* **2014**, *2*, 108.
- [21] M. Rahman, S. Laurent, N. Tawil, Y. L'Hocine, M. Mahmoudi, *Protein-Nanoparticle Interactions*, Springer, Berlin **2013**.
- [22] M. Schäffler, M. Semmler-Behnke, H. Sarioglu, S. Takenaka, A. Wenk, C. Schleh, S. M. Hauck, B. D. Johnston, W. G. Kreyling, *Nanotechnology* **2013**, *24*, 265103.
- [23] E. Casals, T. Pfaller, A. Duschl, G. J. Oostingh, V. F. Puentes, *Small* **2011**, *7*, 3479.
- [24] J. H. Shannahan, J. M. Brown, R. Chen, P. C. Ke, X. Lai, S. Mitra, F. A. Witzmann, *Small* **2013**, *9*, 2171.
- [25] V. Filipe, A. Hawe, W. Jiskoot, *Pharm. Res.* **2010**, *27*, 796.
- [26] B. S. Schuster, L. M. Ensign, D. B. Allan, J. S. Suk, J. Hanes, *Adv. Drug Delivery Rev.* **2015**, *91*, 70.
- [27] S. Palchetti, V. Colapicchioni, L. Digiacomo, G. Caracciolo, D. Pozzi, A. L. Capriotti, G. La Barbera, A. Laganà, *Biochim. Biophys. Acta, Biomembr.* **2016**, *1858*, 189.
- [28] M. Kokkinopoulou, J. Simon, K. Landfester, V. Mailänder, I. Lieberwirth, *Nanoscale* **2017**, *9*, 8858.
- [29] M. J. Hajipour, S. Laurent, A. Aghaie, F. Rezaee, M. Mahmoudi, *Biomater. Sci.* **2014**, *2*, 1210.
- [30] S. Tenzer, D. Docter, J. Kuharev, A. Musyanovych, V. Fetz, R. Hecht, F. Schlenk, D. Fischer, K. Kiouptsi, C. Reinhardt, K. Landfester, H. Schild, M. Maskos, S. K. Knauer, R. H. Stauber, *Nat. Nanotechnol.* **2013**, *8*, 772.
- [31] G. Caracciolo, D. Caputo, D. Pozzi, V. Colapicchioni, R. Coppola, *Colloids Surf., B* **2014**, *123*, 673.
- [32] F. Benetti, M. Fedel, L. Minati, G. Speranza, C. Migliaresi, *J. Nanopart. Res.* **2013**, *15*, 1694.
- [33] A. C. G. Weiss, K. Kempe, S. Förster, F. Caruso, *Biomacromolecules* **2018**, *19*, 2580.
- [34] S. Winzen, S. Schoettler, G. Baier, C. Rosenauer, V. Mailänder, K. Landfester, K. Mohr, *Nanoscale* **2015**, *7*, 2992.
- [35] C. Weber, S. Morsbach, K. Landfester, *Angew. Chem., Int. Ed.* **2019**, *58*, 12787.
- [36] K. Braeckmans, K. Buyens, W. Bouquet, C. Vervaeke, P. Joye, F. D. Vos, L. Plawinski, L. Doeuvre, E. Angles-Cano, N. N. Sanders, J. Demeester, S. C. D. Smedt, *Nano Lett.* **2010**, *10*, 4435.
- [37] M. C. Lo Giudice, L. M. Herda, E. Polo, K. A. Dawson, *Nat. Commun.* **2016**, *7*, 13475.
- [38] R. Frost, C. Langhammer, T. Cedervall, *Nanoscale* **2017**, *9*, 3620.
- [39] M. Lundqvist, J. Stigler, G. Elia, I. Lynch, T. Cedervall, K. A. Dawson, *Proc. Natl. Acad. Sci. USA* **2008**, *105*, 14265.
- [40] T. Cedervall, I. Lynch, M. Foy, T. Berggård, S. C. Donnelly, G. Cagney, S. Linse, K. A. Dawson, *Angew. Chem., Int. Ed.* **2007**, *46*, 5754.
- [41] S. Schöttler, G. Becker, S. Winzen, T. Steinbach, K. Mohr, K. Landfester, V. Mailänder, F. R. Wurm, *Nat. Nanotechnol.* **2016**, *11*, 372.
- [42] G. Settanni, J. Zhou, T. Suo, S. Schöttler, K. Landfester, F. Schmid, V. Mailänder, *Nanoscale* **2017**, *9*, 2138.
- [43] L. Shang, G. U. Nienhaus, *Acc. Chem. Res.* **2017**, *50*, 387.
- [44] S. Milani, F. B. Bombelli, A. S. Pitek, K. A. Dawson, J. Rädler, *ACS Nano* **2012**, *6*, 2541.
- [45] M. Carril, D. Padro, P. Del Pino, C. Carrillo-Carrion, M. Gallego, W. J. Parak, *Nat. Commun.* **2017**, *8*, 1542.
- [46] O. Vilanova, J. J. Mittag, P. M. Kelly, S. Milani, K. A. Dawson, J. O. Rädler, G. Franzese, *ACS Nano* **2016**, *10*, 10842.